J. Chem. Soc., Faraday Trans. 2, 1986, **82**, 1763–1787 (Faraday Symposium 20)

Capillary Condensation and Adsorption in Cylindrical and Slit-like Pores

Robert Evans* and Umberto Marini Bettolo Marconi
H. H. Wills Physics Laboratory, University of Bristol, Bristol BS8 1TL
Pedro Tarazona
Instituto de Fisica del Estado Solido, Facultad de Ciencias, Universidad Autonoma, Madrid 28049, Spain

The nature of adsorption of simple fluids confined in model pores is investigated by means of a density functional approach. For temperatures T corresponding to a partial wetting situation a first-order phase transition (capillary condensation) from dilute 'gas' to dense 'liquid' occurs at relative pressures p/p_{sat} close to those predicted by the macroscopic Kelvin equation, even for radii R_c or wall separations H as small as 10 molecular diameters. In a complete wetting situation, where thick films develop, the Kelvin equation is, in general, not accurate. At fixed T the adsorption $\Gamma_m(p)$ exhibits a loop; Γ_m jumps discontinuously at the first-order transition, but the accompanying metastable portions of the loop could produce hysteresis similar to that observed in adsorption measurements on mesoporous solids. Metastable thick films persist to larger p/p_{sat} in slits than in cylinders and this has repercussions for the shape of hysteresis loops. For a given pore size the loop in Γ_m shrinks with increasing T and disappears at a capillary critical temperature T_c^{cap} ($< T_c$). If $T > T_c^{cap}$ condensation no longer occurs and hysteresis of Γ_m will not be observed. Such behaviour is found in experiments. A prewetting (thick–thin film) transition can occur for confined fluids. The transition is shifted to a smaller value of p/p_{sat} than that appropriate to prewetting at a single planar wall. Whereas the magnitude of the shift is very small for slits, it is substantial for cylinders and this leads to the possibility of finding a triple point, where 'liquid' and thick and thin films coexist, in cylindrical pores whose radii may not be too large for investigation by experiment or computer simulation. Adsorption of supercritical fluids ($T > T_c$, the bulk critical temperature) in cylinders is mentioned briefly.

1. Introduction

The measured adsorption isotherms of gases in mesoporous solids are characterized by steeply varying portions and pronounced hysteresis loops.[1] The increasing (adsorption) part is usually associated with the capillary condensation of the gas to a dense, liquid-like state in the pore, whereas the decreasing (desorption) part is associated with the evaporation of the condensed 'liquid'. Such an interpretation appears to date back to Zsigmondy[2] in 1911. In spite of much subsequent effort[1, 3] the theory of adsorption in solids with narrow pores remains in its infancy. While many of the difficulties in real materials arise from the complex connectivity and topology of the pores and the fact that the pores are not of a uniform size, even the nature of adsorption in the idealized case of a single, infinitely long model pore is poorly understood. Recently we have embarked upon a detailed theoretical investigation of phase equilibria, adsorption and related phenomena for simple fluids confined in slit-like and cylindrical capillaries which act as models for a single pore. Our approach is based on a mean-field density functional

theory of inhomogeneous fluids which treats the solid walls of the capillary as an external potential acting on the fluid molecules. This type of approach has been applied successfully to several interfacial problems. In particular it provides much insight into the factors that determine the systematics of wetting transitions, contact angles and adsorption isotherms at fluid–fluid interfaces and at the interface between a fluid and a single planar wall.[4] Our results suggest that confined fluids can also exhibit rich phase equilibria which are reflected in the calculated adsorption isotherms.

In an earlier paper[5] we focussed attention on a slit-like capillary in which the fluid is confined by two parallel walls of infinite extent.† For a specific choice of fluid–fluid and wall–fluid potential functions we were able to calculate the capillary phase diagram in terms of the variables T (temperature), μ (chemical potential) and H (separation of the walls). In addition, physically transparent formulae for the adsorption and the force acting between the two walls were derived. Here we concentrate rather on cylindrical pores, which are usually considered to be more realistic[1] models for real materials. Cylindrical geometry hinders analytical progress and we are driven to numerical solutions at an earlier stage than for planar (slit) geometry. We find that whilst adsorption in cylinders has many features in common with that in slits there are some important quantitative differences, especially in complete wetting situations where thick liquid films develop on the walls. These differences are particularly relevant for the shape of the adsorption isotherms and for the possible observation of the thick–thin film (prewetting) transition in confined fluids.

Before turning to a microscopic theory for inhomogeneous fluids it is instructive to ask what can be learnt about the phase equilibria of confined fluids from macroscopic (thermodynamic) arguments.[6] We consider two model pores each in contact with a reservoir of fluid at fixed T and μ. The open cylinder is infinitely long ($L \to \infty$) and of interior radius R_c while the slit is as described above. For a given R_c or H the fluid will adopt that configuration which minimizes the grand potential Ω. The latter is conveniently divided into bulk and surface contributions:

$$\Omega = -pV + \gamma A_{sf}$$

where p is the (bulk) pressure corresponding to (μ, T), V is the interior volume and A_{sf} is the total area of the solid–fluid interface. γ is the interfacial free energy or excess grand potential per unit area; it depends on R_c or H. We restrict consideration to $T < T_c$, the bulk critical temperature, and $\mu < \mu_{sat}$, the chemical potential at saturation, so that the fluid in the reservoir is a (bulk) gas.

In the limit R_c or $H \to \infty$ the equilibrium configuration will be 'gas'. Provided the deviation $\Delta\mu = \mu_{sat} - \mu$ is small $\gamma \to \gamma_{sg}$, the solid–gas interfacial tension defined for $\mu = \mu_{sat}$ and $H = \infty$. The grand potential is then $\Omega_g \approx -pV + \gamma_{sg} A_{sf}$. The fluid in the pore may condense to a dense 'liquid' configuration if the walls are sufficiently attractive to fluid molecules and $\Delta\mu$ is not too large. In this case $\gamma \to \gamma_{sl}$, the solid–liquid interfacial tension, again defined for $\mu = \mu_{sat}$ and $H = \infty$. The corresponding grand potential is $\Omega_l \approx -p_l^\dagger V + \gamma_{sl} A_{sf}$, where $p_l^\dagger$ is the pressure of the metastable bulk liquid with density $\rho_l^\dagger$ at the same value of μ. [A van der Waals loop in the (bulk) μ against ρ relation is required.][5] A first-order phase transition from 'gas' to 'liquid' will occur when $\Omega_g - \Omega_l = 0$, or when the pressure p satisfies

$$p - p_l^\dagger = (\gamma_{sg} - \gamma_{sl})\, A_{sf}/V. \tag{1}$$

Introducing Young's equation for the contact angle θ at a single planar wall, $\gamma_{sg} = \gamma_{sl} + \gamma_{lg} \cos\theta$, eqn (1) reduces to

$$p - p_l^\dagger = \begin{cases} 2\gamma_{lg} \cos\theta / R_c & \text{(cylinder)} \quad (2a) \\ 2\gamma_{lg} \cos\theta / H & \text{(slit)} \quad (2b) \end{cases}$$

† Ref. (5) contains a brief review of earlier work on adsorption in model pores and on the phase equilibria of fluids, or magnets, between parallel walls.

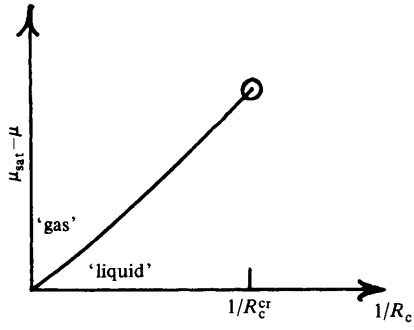

Fig. 1. A schematic capillary coexistence curve for a fluid at fixed temperature. The slope of this curve near the origin is $2\gamma_{lg}\cos\theta/(\rho_l-\rho_g)$. It ends at a critical point at radius R_c^{cr} and chemical potential μ^{cr}.

where γ_{lg} is the (planar) liquid–gas surface tension at temperature T. 'Gas' is stable for values of p smaller, or values of H and R_c larger, than those given by eqn (2), whereas 'liquid' is stable for larger values of p or smaller values of H and R_c. The two configurations coexist when p satisfies eqn (2). The r.h.s. of eqn (2*b*) is simply the macroscopic pressure difference that would arise across the concave cylindrical meniscus between liquid and gas in a vertical slit; the mean radius of curvature entering Laplace's formula is $H/\cos\theta$ and we assume $\theta < \pi/2$. Similarly the r.h.s. of eqn (2*a*) refers to the pressure difference across the hemispherical meniscus in a cylinder; the mean radius of curvature is $R_c/\cos\theta$.

For small undersaturations p and $p_l^\dagger$ can be expanded about p_{sat} and, to first order in $\Delta\mu$, $p-p_l^\dagger = \Delta\mu(\rho_l-\rho_g)$, where ρ_l and ρ_g are the number densities of coexisting liquid and gas. Eqn (2) reduce to the familiar Kelvin equation for capillary condensation if we make the additional assumption that the gas is close to ideal so that

$$kT\ln(p_{sat}/p) \approx \Delta\mu = \begin{cases} 2\gamma_{lg}\cos\theta/R_c(\rho_l-\rho_g) & \text{(cylinder)} \quad (3a) \\ 2\gamma_{lg}\cos\theta/H(\rho_l-\rho_g) & \text{(slit).} \quad (3b) \end{cases}$$

This derivation differs from the conventional argument,[1] which invokes directly the pressure difference across a curved meniscus. It is not necessary to introduce a meniscus into the problem nor it is necessary to introduce specific assumptions about solid–fluid contributions to Ω. Eqn (3) should constitute a rigorous asymptotic result for the condensation pressure in the limits R_c or $H \to \infty$ and $\Delta\mu \to 0$ provided the bulk gas is sufficiently dilute to be treated as ideal. For smaller R_c or H and larger $\Delta\mu$, γ differs significantly from γ_{sg} or γ_{sl}, and eqn (2) and (3) become less accurate. One of the aims of the present work is to determine the regime of validity of these asymptotic results. Note that eqn (3) provides a measure of the shift of the bulk coexistence curve (line of first-order transitions) resulting from confinement of the fluid. This is better illustrated by a capillary phase diagram using $\Delta\mu$ and $1/R_c$ (or $1/H$) as variables. For a given T, coexistence between 'liquid' and 'gas' in the capillary is denoted by a line in the ($\Delta\mu$, $1/R_c$) plane (see fig. 1). This line has a limiting slope $2\gamma_{lg}\cos\theta/(\rho_l-\rho_g)$ as $R_c \to \infty$. We find from our calculations that for sufficiently large $1/R_c$ and $\Delta\mu$ the line of capillary coexistence ends in a capillary critical point beyond which there is only one fluid configuration in the slit. $1/R_c$ plays a role analogous to that of temperature in determining the bulk vapour pressure $p_{sat}(T)$ [or $\mu_{sat}(T)$] curve. A more comprehensive discussion of capillary phase diagrams and critical points can be found in ref. (5).

In deriving eqn (2) we implicitly assumed that the liquid did not wet the walls completely, *i.e.* a partial wetting situation with $\theta > 0$, so that in the limit $\Delta\mu \to 0$ only a thin (microscopic) film of liquid-like density is adsorbed at the walls in the 'gas'

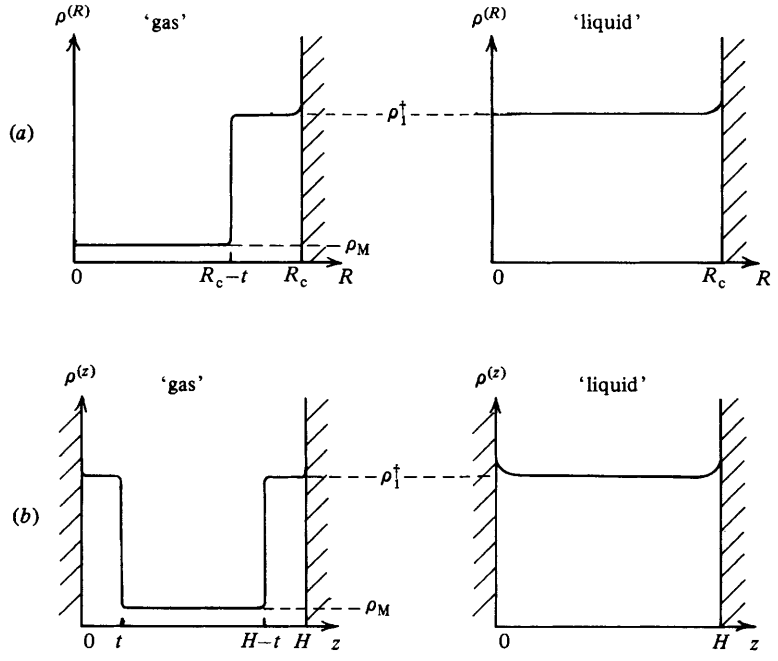

Fig. 2. Schematic density profiles ρ for 'gas' and 'liquid' configurations in a complete wetting situation: (*a*) a cylinder of radius R_c and (*b*) a slit of width H. A wetting film of thickness t develops at the walls for the 'gas'. $\rho_l^\dagger$ is the density of the metastable liquid and ρ_M is the density of the 'gas' at the centre. In the slab approximation the density changes discontinuously at the edge of a film.

configuration. When $\theta = 0$ thick, liquid-like films intrude between the walls and the gas as $\Delta\mu \to 0$, see fig. 2. In the cylinder near $R = R_c - t$ and in the slit near $z = t$ and $z = H - t$, where t is the thickness of a single film, the density profile ρ resembles that of a liquid–gas interface. A crude approximation for the grand potential of such a 'gas' is

$$\Omega_g \approx -pV_g - p_l^\dagger V_l + \gamma_{sl} A_{sl} + \gamma_{lg} A_{lg}$$

where V_g is the volume occupied by gas, V_l the volume occupied by the wetting film of metastable liquid and A_{lg} is the area of the liquid–gas interface. For the cylinder this yields

$$\frac{\Omega_g}{2\pi L} = -\frac{p}{2}(R_c - t)^2 - \frac{p_l^\dagger}{2}(2R_c t - t^2) + R_c \gamma_{sl} + (R_c - t)\gamma_{lg} \tag{4a}$$

while for the slit

$$\frac{\Omega_g}{A_{sl}} = -\frac{p}{2}(H - 2t) - p_l^\dagger t + \gamma_{sl} + \gamma_{lg}. \tag{4b}$$

The grand potential of the 'liquid', whose profile is also shown in fig. 2, is given as previously with $V = V_g + V_l$. Thus condensation occurs when

$$p - p_l^\dagger = \begin{cases} 2\gamma_{lg}/(R_c - t) & \text{(cylinder)} \quad (5a) \\ 2\gamma_{lg}/(H - 2t) & \text{(slit).} \quad (5b) \end{cases}$$

In the limits R_c and $H \to \infty$ these results reduce to those of eqn (2). The r.h.s. of (5*a*) is the Laplace expression for the pressure difference across the hemispherical meniscus whose mean radius of curvature is now $R_c - t$ while the r.h.s. of (5*b*) refers to the cylindrical meniscus of radius $H - 2t$. These modifications to the Kelvin equation were

proposed originally by Cohan.[7] A more systematic treatment of the influence of wetting films was contained in an important early paper by Derjaguin,[8] who showed that the correction to the Kelvin equation depends on the form chosen for the attractive part of the solid–fluid potential function; replacing R_c by $R_c - t$ or H by $H - 2t$ is valid[6] only for exponentially decaying or finite ranged potentials. We return to this point later. Unfortunately the significance of Derjaguin's paper does not appear to have been recognized in the Western literature. Subsequent attempts[1, 3, 9, 10] at improvements on the Kelvin equation have usually been based on semi-empirical arguments and the status of these attempts is rather obscure. Consequently the validity and usefulness of eqn (5) remain uncertain. Formulae of this type are often applied to the hysteresis loops of measured adsorption isotherms. While there is much discussion[1, 3] as to whether they are more appropriate to the adsorption or desorption branches, no systematic investigation of their limitations appears to have been reported. Certainly in the neighbourhood of a capillary critical point, where the distinction between 'liquid' and 'gas' configurations disappears, the Kelvin equation [eqn (3)] or its modification [eqn (5)] will not be applicable.[5] Some microscopic theories have been employed. Calculations for a lattice gas confined between two parallel walls were reported by Hill,[11] who found jumps in the adsorption associated with capillary condensation. He did not make contact with the macroscopic Kelvin equation, however. More detailed mean-field calculations for a lattice gas confined in a single cylindrical pore were performed by Nicholson,[12] who determined a critical radius below which no capillary condensation occurred. Another relevant paper is that of Saam and Cole,[13] who investigated the adsorption of He in a cylindrical pore using a simple model of a continuum fluid.

In this paper we calculate adsorption isotherms for cylinders and slits using the density functional approach. At a first-order transition the adsorption Γ_m jumps by a finite amount. The pressure at which the transition occurs can be compared with that given by eqn (3) and (5) and hence the validity of these formulae can be ascertained. For fixed T and R_c(or H) $\Gamma_m(\mu)$ exhibits a loop. The accompanying metastable states, which would give rise to hysteresis phenomena in a single pore, are examined in some detail.

The remainder of the paper is arranged as follows: in section 2 we outline the density functional approach and describe the potential functions used to model fluid–fluid and wall–fluid interactions. Section 3 contains the results of numerical calculations of adsorption isotherms, illustrating condensation, metastable states and critical points, for a variety of pore sizes, temperatures and wall–fluid potentials. Under certain circumstances the coexistence of thick and thin films (prewetting) can be observed in pores and we give an example of a model system in which coexistence occurs between weakly metastable films; 'liquid' is slightly more stable suggesting that a triple point, where 'thick' and 'thin' films and 'liquid' all coexist, is close. Some results for adsorption from supercritical ($T > T_c$) fluids in cylinders with different radii are also presented. In section 4 we introduce simple slab approximations to the density profiles in order to obtain some explicit formulae for the grand potential of fluid configurations. These formulae allow us to derive instructive analytical results for the thickness and limit of stability of wetting films and provide a self-consistent treatment of capillary condensation, valid in the limit of wide capillaries and thick films. They also provide a useful framework for interpreting the results of our numerical calculations on the prewetting transition and determining the location of capillary critical points. We conclude, in section 5, with a discussion of our results and their possible relevance for adsorption in real mesoporous solids.

2. A Density Functional Theory for Confined Fluids

Any microscopic treatment of adsorption and capillary coexistence must be based on a realistic theory of the inhomogeneous fluid confined in the pore. In particular the theory must describe wetting films and provide a reasonable account of bulk coexistence. The

density functional theory we have employed is based on a simple mean-field approach that has been used in several successful studies of adsorption and wetting transitions at a single wall[4] and of the structure and surface tension of a free liquid–gas interface, where it has been shown[14, 15] to give results in good agreement with those of computer simulation.

We consider a model intrinsic Helmholtz free energy functional

$$\mathscr{F}[\rho] = \int \mathrm{d}\boldsymbol{r}\, f_{\mathrm{h}}[\rho(\boldsymbol{r})] + \frac{1}{2}\iint \mathrm{d}\boldsymbol{r}\,\mathrm{d}\boldsymbol{r}'\, \rho(\boldsymbol{r})\,\rho(\boldsymbol{r}')\, w_2(|\boldsymbol{r}-\boldsymbol{r}|) \tag{6}$$

in which the contribution from repulsive forces between molecules is treated in local density approximation: $f_{\mathrm{h}}(\rho)$ is the Helmholtz free energy density of a uniform hard-sphere fluid of density ρ. The attractive forces are treated in a mean-field or random phase approximation; $w_2(r)$ is the attractive part of the pairwise potential between two fluid molecules. By making a local density approximation we omit the short-ranged correlations[16] arising from packing (excluded volume) effects. This means that the resulting density profiles $\rho(\boldsymbol{r})$ do not exhibit the oscillations which usually occur for fluids near walls. Short-ranged correlations can be included by making a coarse-graining approximation for the hard-sphere free energy functional[17, 18] or by other methods;[19] we comment on the need for such improved treatments later. The equilibrium density profile of the fluid is obtained by minimizing the grand potential functional[20]

$$\Omega_{\mathrm{v}}[\rho] = \mathscr{F}[\rho] - \int \mathrm{d}\boldsymbol{r}\,[\mu - V(\boldsymbol{r})]\,\rho(\boldsymbol{r}) \tag{7}$$

where μ is the chemical potential (fixed by the reservoir) and $V(\boldsymbol{r})$ is the total wall–fluid (external) potential. The minimum value of Ω_{v} is the equilibrium grand potential Ω. Thus $\rho(\boldsymbol{r})$ satisfies

$$\mu = V(\boldsymbol{r}) + \mu_{\mathrm{h}}[\rho(\boldsymbol{r})] + \phi_{\mathrm{eff}}(\boldsymbol{r}) \tag{8}$$

with $\phi_{\mathrm{eff}}(\boldsymbol{r}) \equiv \int \mathrm{d}\boldsymbol{r}' w_2(|\boldsymbol{r}-\boldsymbol{r}'|)\,\rho(\boldsymbol{r}')$, the effective one-body potential arising from attractive fluid–fluid interactions and $\mu_{\mathrm{h}}(\rho) = \mathrm{d}f_{\mathrm{h}}(\rho)/\mathrm{d}\rho$, the local hard-sphere chemical potential. If a molecule in the fluid interacts with a molecule in the wall *via* a Yukawa pairwise potential $-C\exp(-\lambda_{\mathrm{w}} r)/r$, where C and λ_{w} are positive constants, it is straightforward to calculate $V(\boldsymbol{r})$ assuming a constant density n_{w} of wall molecules. For a fluid confined by two parallel walls, unbounded in the x and y directions and separated by a distance H in the z direction, we obtain

$$V(\boldsymbol{r}) \equiv V_{\mathrm{p}}(z) = \begin{cases} -\varepsilon_{\mathrm{w}}\{\exp(-\lambda_{\mathrm{w}} z) + \exp[-\lambda_{\mathrm{w}}(H-z)]\} & 0 < z < H \\ \infty & z < 0;\ z > H. \end{cases} \tag{9}$$

(Each wall is assumed impenetrable.) ε_{w} is a positive strength parameter proportional to Cn_{w}. An external potential of this form was employed in our earlier calculations. Adopting the same procedure for the fluid confined in an infintely long cylindrical capillary of interior radius R_{c} we find, after some algebra

$$V(\boldsymbol{r}) \equiv V_{\mathrm{c}}(R) = \begin{cases} -2\varepsilon_{\mathrm{w}}\lambda_{\mathrm{w}} R_{\mathrm{c}} K_1(\lambda_{\mathrm{w}} R_{\mathrm{c}})\, I_0(\lambda_{\mathrm{w}} R) & R < R_{\mathrm{c}} \\ \infty & R > R_{\mathrm{c}} \end{cases} \tag{10}$$

where R is the radial distance from the axis of the cylinder and I_0 and K_1 are modified Bessel functions.[21] In the limits $R_{\mathrm{c}} \to \infty$ and $R \to \infty$ the product

$$K_1(\lambda_{\mathrm{w}} R_{\mathrm{c}})\, I_0(\lambda_{\mathrm{w}} R) \to \exp[-\lambda_{\mathrm{w}}(R_{\mathrm{c}} - R)]/2\lambda_{\mathrm{w}}(RR_{\mathrm{c}})^{\frac{1}{2}}$$

and

$$V_{\mathrm{c}}(R) \to -\varepsilon_{\mathrm{w}} \exp(-\lambda_{\mathrm{w}} z)$$

provided $z = |R_{\mathrm{c}} - R| \ll R_{\mathrm{c}}$. Thus the cylindrical wall potential reduces to the planar wall potential in the appropriate limit. A plot of $V_{\mathrm{c}}(R)$ is shown in fig. 3; it is somewhat deeper than $V_{\mathrm{p}}(z)$ for a given ε_{w}.

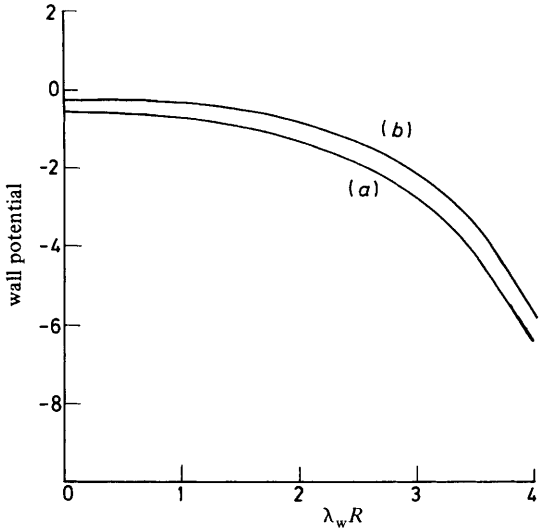

Fig. 3. Comparison of attractive wall potentials: (*a*) $V_c(R)$ for a cylinder of radius $\lambda_w R_c = 4$ and (*b*) $V_p(\lambda_w z)$ for a slit of width $\lambda_w H = 8$. Here $\lambda_w z = \lambda_w H/2 + \lambda_w R$. In each case $\varepsilon_w = 5.625$.

If the attractive fluid–fluid potential is also taken to be a Yukawa:

$$w_2(r) = -\alpha\lambda^3 \exp(-\lambda r)/4\pi\lambda r \tag{11}$$

where $\alpha = -\int \mathrm{d}\boldsymbol{r}\, w_2(r)$ is the integrated strength, $\phi_{\mathrm{eff}}(\boldsymbol{r})$ can be reduced to one-dimensional integrals. In the planar case

$$\phi_{\mathrm{eff}}(z) = -\frac{\alpha}{2}\lambda \int_0^H \mathrm{d}z' \rho(z') \exp(-\lambda|z-z'|) \tag{12}$$

whereas in the cylindrical case

$$\phi_{\mathrm{eff}}(R) = -\lambda^2\alpha K_0(\lambda R)\int_0^R \mathrm{d}R'\, R'\, I_0(\lambda R')\,\rho(R') - \lambda^2\alpha I_0(\lambda R)\int_R^{R_c} \mathrm{d}R'\, R'\, K_0(\lambda R')\,\rho(R'). \tag{13}$$

This last result may be obtained by expanding the Yukawa in a series of products of modified Bessel functions $I_m K_m$ (m is an integer); only the $m = 0$ terms remain when the appropriate integration is performed (see Appendix 1). In the special case where $\lambda_w = \lambda$, so that the decay lengths of the attractive wall–fluid and fluid–fluid potentials are the same, the integral eqn (8) can be transformed into a non-linear differential equation for $\rho(\boldsymbol{r}) \equiv \rho(z)$ (planar) or $\rho(\boldsymbol{r}) \equiv \rho(R)$ (cylinder). This model and procedure were developed originally by Sullivan[16] for a single planar wall and extended later to the two-wall problem.[5] In these planar cases the second-order differential equation possesses an explicit first integral and the solutions are easily determined. However, for the cylindrical case no explicit first integral exists and we found it more convenient to solve the integral equation

$$\mu = V_c(R) + \mu_h[\rho(R)] + \phi_{\mathrm{eff}}(R) \tag{14}$$

with V_c from eqn (10) and ϕ_{eff} given by eqn (13), using a simple iteration scheme.[22] One makes some initial estimate $\rho_i(R)$ and computes

$$\mu_h[\rho_{i+1}(R)] = \mu - V_c(R) - \phi_{\mathrm{eff}}(\rho_i; R).$$

This generates $\rho_{i+1}(R)$ since $\mu_h(\rho)$ is a monotonically increasing function of ρ. The convergence of the solution is usually rapid and corresponds to the approach to a local minimum of the grand potential Ω. To obtain solutions with thick wetting films we found

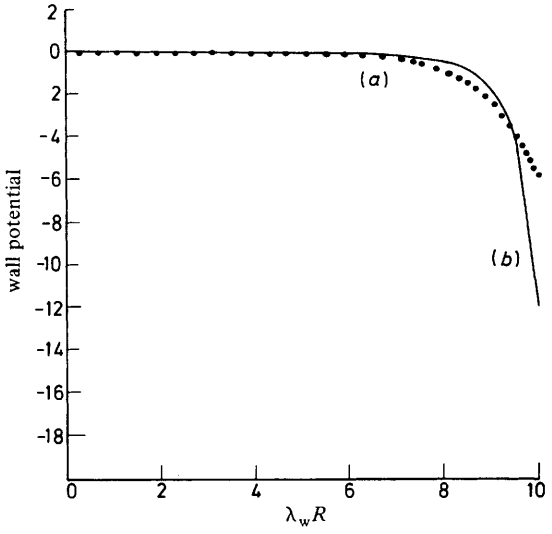

Fig. 4. Comparison of the Yukawa and van der Waals-based wall potentials for cylinders: (*a*) $V_c(\lambda_w R)$ for a cylinder of radius $\lambda_w R_c = 10$ and (*b*) $V_{cvw}(\lambda_w R)$ for a radius $\lambda_w R_c = 11$, constructed as described in Appendix 2 with $\sigma_w = \lambda_w^{-1}$ and $\varepsilon_w = 5.625$.

it necessary to generate initial profiles for $\mu > \mu_{sat}$. These were then used as trial functions for the iteration scheme at $\mu < \mu_{sat}$. Nevertheless, the procedure is usually more efficient than a single planar wall[22] where one must ensure that solution merges smoothly into the bulk fluid. In most of the calculations reported here we set $\lambda_w = \lambda$. For a single planar wall this choice ensures that the wetting transition is second order (critical)[23] with no accompanying thick–thin film (prewetting) transition.[4] In order that we might investigate the latter in cylindrical geometry we also performed calculations for a model with $\lambda_w = 0.8\,\lambda$.[22]

A more realistic wall–fluid potential should take into account the long-ranged attractive van der Waals or London forces. The resulting algebraic decay of the potential is known to be important in determining the growth of wetting films[8] and the character of the wetting transition at a single planar wall.[22, 24] Recently we argued[6] that the same algebraic decay should give rise to significant effects in capillary condensation when the pore is wide and the gas is weakly undersaturated so that thick wetting films of liquid develop on the walls. A suitable model potential can be constructed by assuming that a molecule in the fluid interacts with a wall molecule *via* a pairwise potential $-Ar^{-6}$, where A is a positive constant. The details of the construction are given in Appendix 2. In fig. 4 we plot the resulting potential for a cylinder and compare with the corresponding result [eqn (10)] derived from the Yukawa pairwise potential. The van der Waals potential $V_{cvw}(R)$ is substantially deeper than $V_c(R)$ for radii R close to R_c, *i.e.* near the wall, but it is shallower near the centre of the pore. A few density functional calculations were performed for a Yukawa fluid confined by both potentials in order to examine the sensitivity of the results to the form of the wall–fluid potential.

3. Results of Calculations

All our calculations were based on the Carnahan and Starling equation of state for hard spheres. The bulk pressure and chemical potential of the Yukawa fluid as a function

of bulk density ρ_b follow from eqn (6) and (11):

$$p(\rho_b) = p_h(\rho_b) - \alpha\rho_b^2/2 \tag{15}$$

and

$$\mu(\rho_b) = \mu_h(\rho_b) - \alpha\rho_b.$$

The bulk coexisting densities ρ_l and ρ_g are easily obtained from these equations and the critical density ρ_c and temperature T_c satisfy[16]

$$\rho_c d^3 = 0.249; \quad \alpha = 11.102\, kT_c d^3$$

where d is the hard-sphere diameter.

For given μ and T, density profiles $\rho(R)$ corresponding to 'liquid' and 'gas' solutions could usually be found, except for small radii and large undersaturations, where only one solution exists. When two solutions are present, that with the lower grand potential is the stable one; the other corresponds to a metastable solution. If two distinct solutions have equal grand potential for fixed μ and T, 'liquid' and 'gas' coexist in the pore. A capillary critical point occurs when the two hitherto distinct fluid configurations, characterized by distinct density profiles, become indistinguishable. The terms 'liquid' and 'gas' become less appropriate in the approach to such a critical point. When prewetting occurs in a capillary, three solutions, corresponding to 'gas' with distinct thick and thin films and to 'liquid', are present. Examples are given which illustrate these various features.

We found it convenient to construct adsorption isotherms by computing a dimensionless measure of the adsorption or coverage defined by

$$\Gamma_m \equiv \frac{2d^3}{R_c^2}\int_0^{R_c} dR\, R\rho(R) \tag{16a}$$

for the cylinder, or

$$\Gamma_m \equiv \frac{d^3}{H}\int_0^{H} dz\, \rho(z) \tag{16b}$$

for the slit. Γ_m was calculated as a function of the ratio ρ_b/ρ_g, where ρ_b is the bulk gas density at chemical potential $\mu < \mu_{sat}$ and ρ_g is its density at saturation. Results for a partial wetting situation at $T = 0.6T_c$ are shown in fig. 5. The wall potentials are given by eqn (9) or (10) with $\varepsilon_w = 2.114\, kT_c$ and $\lambda_w = \lambda$. For this choice of ε_w the second-order wetting transition at a single planar wall occurs[16] at $T_w = 0.96T_c$. Thus $T \ll T_w$ and the contact angle $\theta \to \pi/2$ so that no thick wetting films develop in the 'gas' solution. At large undersaturations (small ρ_b/ρ_g) Γ_m is small, as is characteristic of adsorption from a dilute 'gas'. A vertical jump in Γ_m occurs at an undersaturation ratio $\rho' \equiv \rho_b'/\rho_g = \rho_{cond}'$. This corresponds to capillary condensation to a dense 'liquid' with large Γ_m, stable for $\rho' > \rho_{cond}'$. ρ_{cond}' varies with R_c (or H). The larger R_c, the larger is ρ_{cond}' and the larger is the jump in Γ_m. For $\lambda R_c = 10$ and 15 the values of ρ_{cond}' (marked by vertical arrows) obtained from the macroscopic Kelvin equation [eqn (3)] are within 1% of the calculated values. However, for the smallest radius, $\lambda R_c = 4$, ρ_{cond}' is significantly smaller than the Kelvin estimate. The adsorption isotherm for the slit with $\lambda H = 4$ is similar to that for $\lambda R_c = 4$; capillary condensation occurs within 1% of that for the cylinder and the magnitude of the jump in Γ_m is almost identical. We note that the metastable ($\rho' < \rho_{cond}'$) portions of the 'liquid' branch of the isotherms extend to rather large undersaturations. The metastable portions of the 'gas' branch extend to large supersaturations $\mu > \mu_{sat}$ or $\rho' > 1$. This is not shown in the figure.

Results for a complete wetting situation are shown in fig. 6. The attractive wall potential is stronger now: $\varepsilon_w = 4.5\, kT_c(\lambda_w = \lambda)$ and the temperature $T = 0.6\, T_c$ lies above the wetting transition temperature $T_w \approx 0.57\, T_c$. The isotherms for the cylinder and the slit are now quite different especially on the 'gas' branches, which now exhibit wetting films.

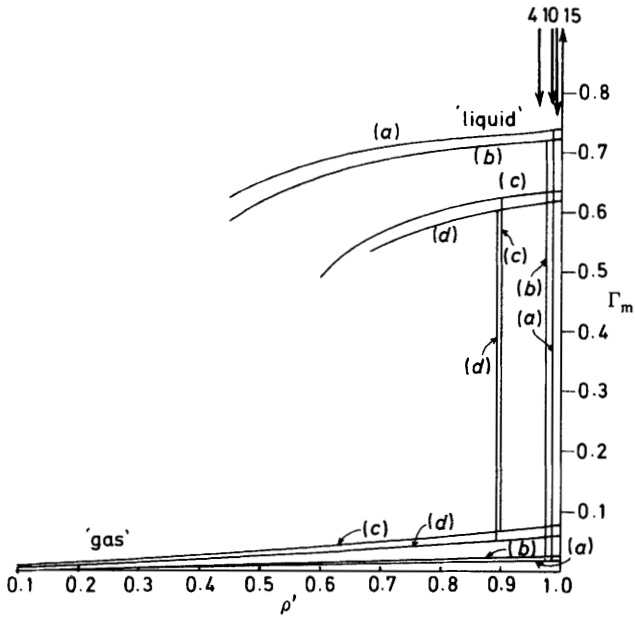

Fig. 5. Adsorption Γ_m plotted against undersaturation ratio $\rho' \equiv \rho_b/\rho_g$ for cylinders and a slit at a fixed temperature $T = 0.6\ T_c$, below T_w. (*a*) $\lambda R_c = 15$, (*b*) $\lambda R_c = 10$, (*c*) $\lambda R_c = 4$ and (*d*) $\lambda H = 4$. The vertical portions represent the jump in Γ_m at the first-order transition (condensation). The vertical arrows mark the undersaturation ratios for which condensation is predicted by the Kelvin equation. Note the large metastable portion of Γ_m on the 'liquid' branch. The metastable portions on the 'gas' branch extend to $\rho' > 1$. $\varepsilon_w = 2.114\ kT_c$.

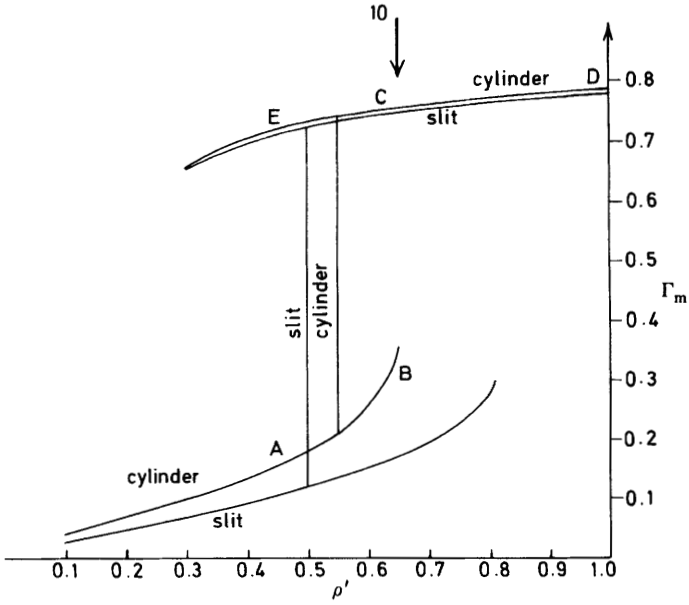

Fig. 6. Adsorption for a cylinder of radius $\lambda R_c = 10$ and a slit of width $\lambda H = 10$ at a temperature $T = 0.6\ T_c$, above T_w. Condensation occurs (vertical portion) at larger undersaturations than that predicted by the Kelvin equation (vertical arrow). The metastable portions on the 'gas' branch now terminate at $\rho' < 1$. $\varepsilon_w = 4.5\ kT_c$.

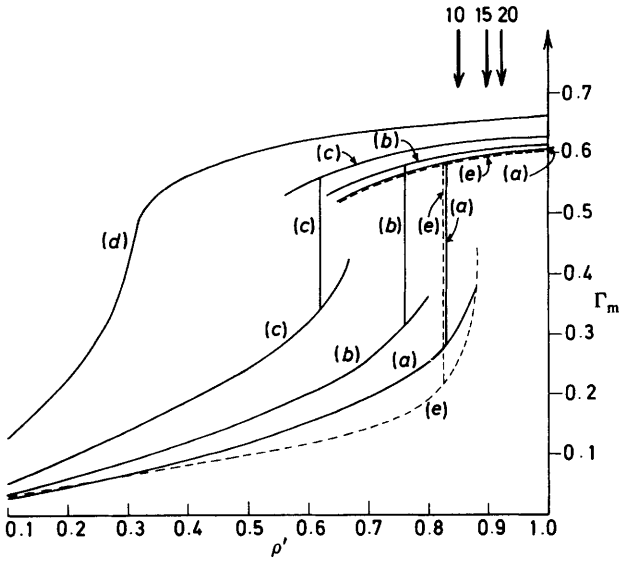

Fig. 7. Adsorption for cylinders at a temperature $T = 0.8\ T_c$, above T_w. Curves (*a*) $\lambda R_c = 20$, (*b*) $\lambda R_c = 15$, (*c*) $\lambda R_c = 10$ and (*d*) $\lambda R_c = 5$ are calculated for the wall potential V_c while (*e*) (dashed line) is calculated for the van der Waals wall potential V_{cvw} constructed as described in Appendix 2 with $\lambda_w R_c = 21$, $\sigma_w = \lambda_w^{-1} = \lambda^{-1}$. The vertical arrows mark the Kelvin estimates for condensation. Curve (*d*) is supercritical. $\varepsilon_w = 4.5\ kT_c$.

Γ_m is larger for the cylinder but the metastable 'gas' portion extends to a limiting undersaturation ratio ρ_1' that is much smaller than the corresponding quantity for the slit. This is a general feature for wetting situations which is accounted for in the next section. The 'gas' branch must terminate[5] at $\rho_1' < 1$ if $T > T_w$ and no prewetting occurs. Capillary condensation occurs at a substantially smaller value of ρ_{cond}' in the slit. The unmodified Kelvin equation [eqn (3)] predicts the same value for the slit and cylinder and this is much too large. We should contrast these results with those for $\lambda R_c = 10$ and 15 shown for a partial wetting case in fig. 5. There, cylinders and slits have almost identical values of ρ_{cond}' and these lie very close to the Kelvin estimate. The modified Kelvin equations [eqn (5)] are not inconsistent with our results, but since $\rho_{cond}' \ll 1$, very thick films do not develop at condensation so [eqn (5)] cannot be used for quantitative purposes.

In fig. 7 results for the same wall potential, but a higher temperature $T/T_c = 0.8$, are plotted for several cylindrial pores. Condensation occurs for the three largest radii, but for $\lambda R_c = 5$, Γ_m increases monotonically with increasing ρ_b/ρ_g. As R_c is reduced the metastable portions of the isotherms shrink and the jump in Γ_m is reduced. Eventually a critical radius is reached for which the loop in Γ_m disappears and $(\partial\mu/\partial\Gamma_m) = (\partial^2\mu/\partial\Gamma_m^2) = 0$. This corresponds to a capillary critical point.[5] In the present case the critical radius is $\lambda R_c \approx 6$. For smaller radii, no first-order transitions occur and only one solution exists. The isotherm for $\lambda R_c = 5$ can therefore be considered supercritical. The Kelvin estimates are poor even for the largest radius $\lambda R_c = 20$. For this case we have compared the results with those obtained using the van der Waals wall potential described in Appendix 2 and plotted (for a smaller radius) in fig. 4. The adsorption on the 'liquid' branch is almost identical to that obtained from the wall potential based on the Yukawa model, but it is lower on the stable 'gas' branch and increases more rapidly on the metastable portion. Condensation occurs at a very slightly

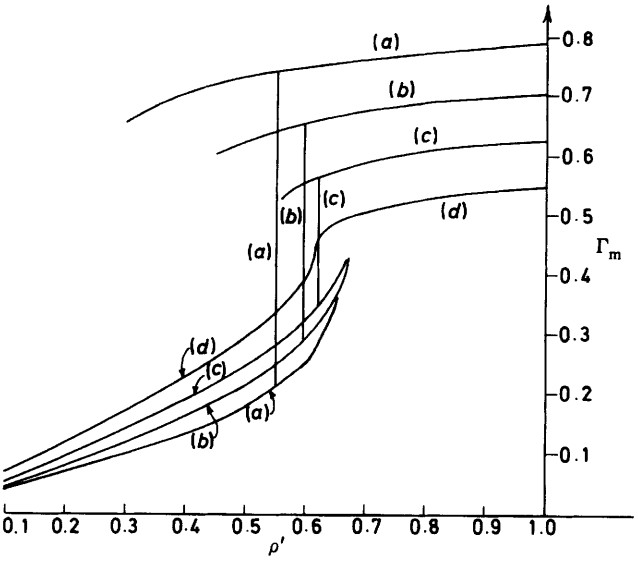

Fig. 8. Adsorption isotherms for a cylinder of radius $\lambda R_c = 10$. (*a*) $T = 0.6\ T_c$, (*b*) $T = 0.7\ T_c$, (*c*) $T = 0.8\ T_c$ and (*d*) $T = 0.9\ T_c$. The vertical portions represent the jump in Γ_m at condensation. Curve (*d*) is slightly supercritical. $\varepsilon_w = 4.5\ kT_c$.

larger undersaturation (smaller ρ') for the van der Waals potential. However ρ'_{cond} is again too small for approximations such as eqn (5) to be reliable.

When making adsorption measurements on mesoporous solids one is not usually at liberty to vary the pore radius. Consequently in making comparison with experiment it is more natural to plot isotherms for different temperatures and fixed radius. Such a plot is given in fig. 8 for the wall potential eqn (10) with $\varepsilon_w = 4.5\ kT_c(\lambda_w = \lambda)$ and $\lambda R_c = 10$. Condensation occurs for the three lowest temperatures but the 'loops' in Γ_m shrink as $T \to T_c$, and for $T \approx 0.9\ T_c$ a capillary point occurs for this choice of R_c. (The isotherm for $T = 0.9\ T_c$ is only slightly supercritical.) For $T \geqslant 0.9\ T_c$ Γ_m increases monotonically with ρ' and no metastable states exist.

In fig. 9 we plot adsorption results for a wall potential that has $\lambda_w = 0.8\ \lambda$, $\lambda = d^{-1}$ and $\varepsilon_w = 3\ kT_c$. As mentioned earlier this model was shown[22] to exhibit a first-order wetting transition at $T_w = 0.58\ T_c$ for a single planar wall. The associated prewetting line, where thick and thin films coexist, extends[22] to the surface critical point at $T_{sc} = 0.645\ T_c$. This line lies very close to the bulk coexistence curve, which it meets tangentially at $T = T_w$. In an earlier paper,[25] we argued that coexistence between stable thick and thin films would only occur in a slit-like capillary if the wall separation H was very large, typically $\approx 70\ d$. For smaller H, condensation will occur at larger undersaturations than prewetting and the latter can only arise as a transition between metastable states. Here we investigate the competition between capillary condensation and prewetting in both slits and cylinders, at a temperature $T = 0.63\ T_c$. For λR_c and $\lambda H = 16$ no prewetting is obtained and capillary condensation occurs at similar values of ρ'_{cond}; both somewhat lower than the estimate from the unmodified Kelvin equation [eqn (3)]. For the larger pores, λR_c and $\lambda H = 30$, prewetting is found, *i.e.* coexistence between two distinct 'gas' configurations corresponding to large and small values of Γ_m. In the slit, prewetting occurs at $\rho'_{pw} = 0.960$, which is very slightly less than the corresponding ratio for a single wall at the same temperature, *i.e.* 0.962. However, the coexisting thick and thin films have a much higher grand potential than the 'liquid' which is the stable configuration

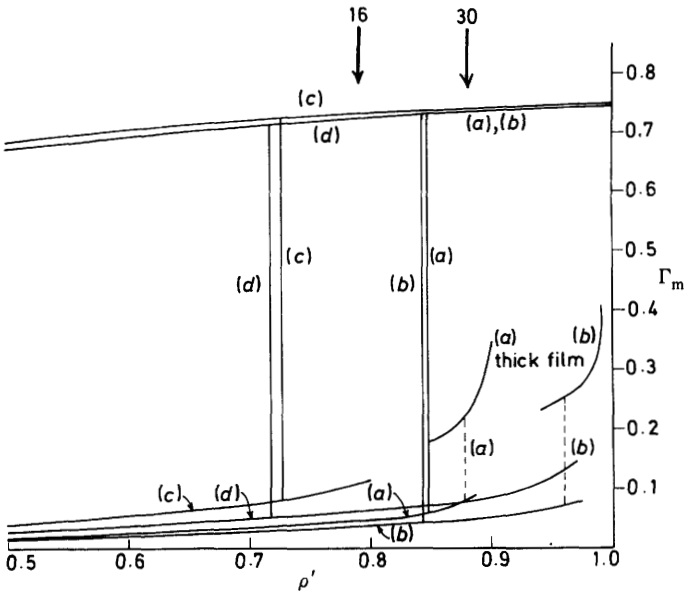

Fig. 9. Adsorption for cylinders and slits at $T = 0.63\ T_c$ for a system that undergoes a first-order wetting transition. (*a*) $\lambda R_c = 30$, (*b*) $\lambda H = 30$, (*c*) $\lambda R_c = 16$ and (*d*) $\lambda H = 16$. (The 'liquid' branch of Γ_m is almost identical for $\lambda R_c = 30$, $\lambda H = 30$ and $\lambda H = 16$.) The vertical portions represent the jump in Γ_m at capillary condensation. For $\lambda R_c = 30$ and $\lambda H = 30$ a prewetting transition (dashed vertical lines) occurs between metastable thick and thin films. The vertical arrows mark the Kelvin estimates for condensation. $\varepsilon_w = 3.0\ kT_c$, $\lambda_w = 0.8\ \lambda$ and $\lambda = d^{-1}$.

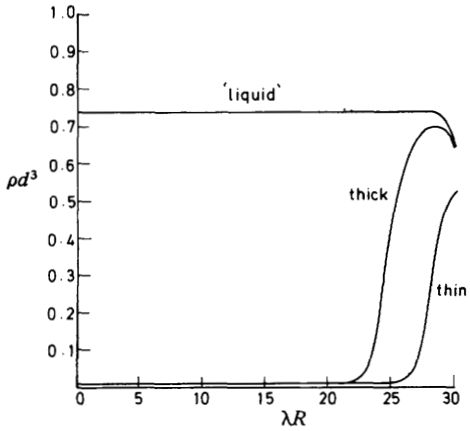

Fig. 10. Density profiles ρ, in reduced units, of 'liquid' and of thick and thin films calculated for a cylinder of radius $\lambda R_c = 30$ at $T = 0.63\ T_c$. See text for details.

for $\rho' > \rho'_{cond} = 0.844$. The case of the cylinder is rather different. Prewetting now occurs at $\rho'_{pw} = 0.878$, well below the result for the slit, and closer to $\rho'_{cond} = 0.848$. Indeed the 'liquid' has only a slightly lower grand potential at ρ'_{pw}. In fig. 10 we plot the density profiles of the three configurations that exist in the cylinder at $\rho' = 0.88$, where the thick and thin films are still very weakly metastable. The 'liquid' density profile is constant throughout the cylinder apart from a decreasing portion very close to the wall. Whereas

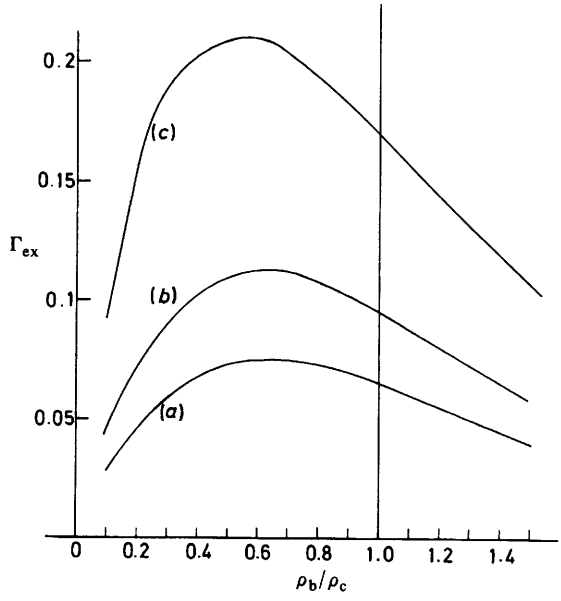

Fig. 11. Adsorption excess Γ_{ex} plotted against ρ_b/ρ_c in cylinders for a supercritical fluid at $T = 1.35\ T_c$. (*a*) $\lambda R_c = 15$, (*b*) $\lambda R_c = 10$ and (*c*) $\lambda R_c = 5$. $\varepsilon_w = 4.5\ \boldsymbol{k}T_c$.

it is likely that with more effort we could find a radius $R_{c\,\mathrm{triple}}$, close to $R_c = 30\ d$, for which 'liquid', thick and thin films would all coexist, such a triple point will only occur in slits at $H_{\mathrm{triple}} \gg 30\ d$. An explanation of this difference is provided in the next section.

Finally, in fig. 11 we present some results for adsorption from supercritical fluids. These refer to cylinders with three different radii and fixed temperature $T = 1.35\ T_c$. The wall potential is given by eqn (10) ($\varepsilon_w = 4.5\ \boldsymbol{k}T_c$ and $\lambda_w = \lambda$). We have chosen to plot the normalized adsorption excess

$$\Gamma_{ex} \equiv \frac{2d^3}{R_c^2} \int_0^{R_c} \mathrm{d}R\ R[\rho(R) - \rho_b]$$

for different ratios ρ_b/ρ_c. Here ρ_b is the bulk fluid density at chemical potential μ and ρ_c is the bulk critical density $\rho_c d^3 = 0.249$. The interesting feature is that Γ_{ex} exhibits a maximum for $\rho_b/\rho_c < 1$ that becomes more pronounced and shifts to smaller values as R_c is reduced. Results similar to those shown in fig. 11 were also obtained for the slit-like capillary. Recently van Megen and Snook[26] performed grand canonical Monte Carlo simulations of supercritical fluids confined between two parallel walls. Their results (see fig. 5 of their paper) exhibit the same trends as ours. A maximum at $\rho_b/\rho_c < 1$ was found in the adsorption excess measurements of Specovious and Findenegg[27] on supercritical ethylene adsorbed on graphitized carbon black. We postpone comparison with these results and detailed discussion of finite size and geometrical effects for near-critical and supercritical fluids to a future paper.

4. The Slab Approximation and its Consequences

Several of the results obtained from the numerical calculations of the last section can be understood in terms of a slab approximation to the density profile of the fluid in the pore. By choosing simple parametrized forms for the profile, explicit expressions for the

grand potential are obtained that can be minimized to obtain equilibrium configurations. The resulting formulae for the thickness of wetting films and for the pressure at which condensation occurs shed much insight into capillary phenomena. Whilst this type of approach is in a similar spirit to that introduced by Derjaguin,[8, 28] and by Frenkel, Halsey and Hill in their slab theory of multilayer adsorption, we employ the density functional formalism to obtain the grand potential as a function of suitable parameters rather than model directly the disjoining pressure.

We concentrate on a 'gas' configuration with a wetting film of thickness t (see fig. 2). The density profile is approximated by

$$\rho(R) = \begin{cases} \rho_M & 0 \leqslant R \leqslant R_c - t \\ \rho_l^\dagger & R_c - t < R \leqslant R_c \end{cases} \tag{17}$$

where $\rho_l^\dagger$ is the density of the metastable bulk liquid at chemical potential μ and temperature T and $\rho_M \equiv \rho(0)$ is the density at the centre. In the present version of the approximation we set $\rho_M = \rho_b$, the density of the bulk gas at $\mu(< \mu_{sat})$ and T. Although this is adequate for large radii R_c and small undersaturations it is not appropriate for the small radii and large undersaturations which are relevant near capillary critical points and a different approximation will be adopted for that case. The grand potential $\Omega_g(t)$ of the 'gas' configuration is obtained by substituting eqn (17) into eqn (6) and (7):

$$\frac{\Omega_g(t)}{2\pi L} = \tfrac{1}{2}[R_c^2 - (R_c - t)^2][f_h(\rho_l^\dagger) - \mu\rho_l^\dagger] + \tfrac{1}{2}(R_c - t)^2[f_h(\rho_b) - \mu\rho_b]$$
$$+ \frac{1}{2}\int_0^{R_c} dR\, R\rho(R) \int dr'\, \rho(R')\, w_2(|r - r'|) + \int_0^{R_c} dR\, R\rho(R)\, V_c(R)$$

where L is the length of the cylinder. Recalling that

$$f_h(\rho_b) = -p_h(\rho_b) + \rho_b \mu_h(\rho_b)$$

assuming the Yukawa eqn (11) for w_2 and using eqn (15), this can be re-written as

$$\frac{\Omega_g(t)}{2\pi L} = \tfrac{1}{2}(2R_c t - t^2)(-\rho_l^\dagger + \alpha\rho_l^{\dagger 2}/2) + \tfrac{1}{2}(R_c - t)^2(-p + \alpha\rho_b^2/2)$$
$$- \frac{\alpha}{2}\int_0^{R_c} dR\, R\rho(R) \int dr'\, \rho(R') \frac{\lambda^3 \exp(-\lambda|r - r'|)}{4\pi\lambda|r - r'|} + \int_0^{R_c} dR\, R\rho(R)\, V_c(R). \tag{18}$$

The double integral can be evaluated using eqn (A 3) and some standard properties[21] of modified Bessel functions. It reduces to

$$-\frac{\alpha}{4}\rho_l^{\dagger 2}(2R_c t - t^2) - \frac{\alpha}{4}\rho_b^2(R_c - t)^2 + \frac{\alpha}{2}\rho_b^2(R_c - t)^2 I_1(\lambda(R_c - t))\, K_1(\lambda(R_c - t))$$
$$+ \frac{\alpha}{2}\rho_l^{\dagger 2}\{R_c^2 K_1(\lambda R_c) I_1(\lambda R_c) + (R_c - t)^2 K_1(\lambda(R_c - t)) I_1(\lambda(R_c - t))$$
$$- 2(R_c - t) R_c K_1(\lambda R_c) I_1(\lambda(R_c - t))\}$$
$$- \alpha\rho_b\rho_l^\dagger \{(R_c - t)^2 I_1(\lambda(R_c - t)) K_1(\lambda(R_c - t)) - (R_c - t) R_c I_1(\lambda(R_c - t)) K_1(\lambda R_c)\}.$$

Choosing eqn (10) for $V_c(R)$ the last term in eqn (18) reduces to

$$-2\varepsilon_w \rho_b R_c(R_c - t) K_1(\lambda_w R_c) I_1(\lambda_w(R_c - t))$$
$$- 2\varepsilon_w \rho_l^\dagger R_c K_1(\lambda_w R_c)\{R_c I_1(\lambda_w R_c) - (R_c - t) I_1(\lambda_w(R_c - t))\}.$$

Combining terms and using the asymptotic expansions[21] ($z \gg 1$) of $I_1(z)$ and $K_1(z)$ we find, to first order in t/R_c,

$$\frac{\Omega_g(t)}{2\pi L} = -\frac{p}{2}R_c^2 + \tfrac{1}{2}(p-p_l^\dagger)(2R_c t - t^2) + \frac{\alpha}{4\lambda}\rho_b^2 R_c(1-t/R_c) + \frac{\alpha}{2\lambda}\rho_l^{\dagger 2}R_c(1-t/2R_c)$$

$$\times[1-\exp(-\lambda t)] - \frac{\alpha}{2\lambda}\rho_b\rho_l^\dagger R_c[(1-t/R_c)-(1-t/2R_c)]\exp(-\lambda t)$$

$$+\frac{\varepsilon_w}{\lambda_w}(\rho_l^\dagger-\rho_b)R_c(1-t/2R_c)\exp(-\lambda_w t) - \frac{\varepsilon_w}{\lambda_w}\rho_l^\dagger R_c. \tag{19}$$

The equilibrium film thickness t_0 is given by differentiating this expression and satisfies

$$(p-p_l^\dagger)(R_c-t_0) = \frac{\alpha}{4\lambda}(\rho_l^\dagger-\rho_b)^2 + (\rho_l^\dagger-\rho_b)\left(\varepsilon_w - \frac{\alpha}{2}\rho_l^\dagger\right)[R_c - \tfrac{1}{2}(t_0-\lambda^{-1})]\exp(-\lambda t_0) \tag{20}$$

where for convenience we have set $\lambda_w = \lambda$. In the limit $\mu \to \mu_{sat}$ we can replace $\rho_l^\dagger$ by ρ_l and ρ_b by ρ_g. The first term of the r.h.s. of eqn (20) is then γ_{lg}, the surface tension of the corresponding slab approximation to the planar liquid–gas interface. The latter is defined by $\rho(z) = \rho_l$, $z < 0$ and $\rho(z) = \rho_g$, $z > 0$; γ_{lg} is the surface excess grand potential per unit area.† Thus eqn (20) reduces to

$$\lambda t_0 = -\ln\left(\frac{p-p_l^\dagger - \gamma_{lg}/(R_c-t_0)}{(\rho_l-\rho_g)(\varepsilon_w - \alpha\rho_l/2)}\right) \tag{21}$$

where we have ignored a term $O(t_0/R_c)$ inside the logarithm and assumed $2\varepsilon_w > \alpha\rho_l$, as is appropriate to complete wetting. This result is significantly different from that obtained from the corresponding analysis for a slit, *i.e.*

$$\lambda t_0 = -\ln\left(\frac{p-p_l^\dagger}{(\rho_l-\rho_g)(\varepsilon_w-\alpha\rho_l/2)\{1+\exp[-\lambda(H-2t_0)]\}}\right). \tag{22}$$

If $H \gg 2t_0$ the equilibrium thickness approaches that of a film at a single planar wall $t_0(\infty)$. Since the correction term is an exponential, films in slits are only slightly thicker than $t_0(\infty)$ for the same undersaturation.[28] In the cylinder, however, the correction to $t_0(\infty)$ depends on the mean radius of curvature $R_c - t_0$; the effective undersaturation $p-p_l^\dagger$ is reduced by an amount $\gamma_{lg}/(R_c-t_0)$. This can be a very substantial quantity, especially at low temperatures where γ_{lg} is large, leading to much thicker films in cylinders. Recall that fig. 6 and 9 show that Γ_m is generally much larger for the 'gas' branch of cylinders than for slits. Moreover eqn (21) indicates that a minimum of $\Omega_g(t)$ can only occur provided $p-p_l^\dagger > \gamma_{lg}/(R_c-t_0)$, a condition which places an implicit lower bound on the undersaturation $p-p_l^\dagger$, below which no thick films can exist. By contrast, the lower bound for the slit is determined by exponential terms and is therefore much smaller than in the cylinder (for $H = R_c$). This argument explains why the adsorption isotherms plotted in fig. 6 and 9 have metastable 'gas' branches extending to much larger ratios p' in slits than in cylinders. It can be understood more clearly by considering the increase in grand

† The result from the slab approximation $\gamma_{lg} = \alpha(\rho_l-\rho_g)^2/4\lambda$ provides a poor estimate of the exact surface tension calculated from the exact solution of eqn (8) for the case $V_p(z) = 0$. This is not important for the present derivation, however. The final formulae are not restricted to the slab approximation and should be utilized with the exact surface tension.

potential associated with an increase δt is the thickness t of the film. We can rewrite eqn (19) as

$$\omega^{ex}(t) \equiv \frac{\Omega_g(t)+\pi L R_c^2 p}{2\pi L R_c} = \frac{1}{2R_c}(p-p_l^\dagger)(2R_c t - t^2) - \gamma_{lg}\frac{t}{R_c} + \Delta\omega(t) \tag{23}$$

where $\Delta\omega(t)$ includes constant terms and terms proportional to $\exp(-\lambda t)$ and $\exp(-\lambda_w t)$. [These exponential terms are omitted in the macroscopic approximation (4*a*).] The increase in surface excess grand potential per unit area of wall, ω^{ex}, on increasing t by an infinitesimal amount δt is $[(p-p_l^\dagger)(1-t/R_c)-\gamma_{lg}/R_c]\,\delta t$ + exponental terms. By contrast the slit has

$$\omega^{ex}(t) \equiv \frac{\Omega_g(t)+A_{sf}Hp}{A_{sf}} = (p-p_l^\dagger)\,t + \Delta\omega(t) \tag{24}$$

and the analogous calculation yields an increase of $(p-p_l^\dagger)\,\delta t$ + exponential terms. While these results agree in the limit $R_c = H \to \infty$, they differ substantially at finite R_c or H. In the cylinder, the increase in ω^{ex} arising from the increase in volume of the metastable 'liquid' constituting the film is moderated by the reduction $(-\gamma_{lg}\delta t/R_c)$ arising from the decrease in area of the 'liquid'–'gas' interface. No such surface (or curvature) effect arises for the slit since the interfacial area is always fixed. The increase in ω^{ex} is positive, and the film stable or metastable provided $p-p_l^\dagger > \gamma_{lg}/(R_c-t)$, the same condition we derived above.

Condensation occurs when $\Omega_g(t_0) = \Omega_l$, the grand potential corresponding to a 'liquid' configuration. The slab approximation sets $\rho(R) = \rho_l^\dagger$ for $0 \leqslant R \leqslant R_c$. It follows that in the limits λR_c and $\lambda_w R_c \gg 1$

$$\frac{\Omega_l}{2\pi L} = -\tfrac{1}{2}p_l^\dagger R_c^2 + \left(\frac{\alpha\rho_l^\dagger}{4\lambda} - \frac{\varepsilon_w}{\lambda_w}\right) R_c \rho_l^\dagger. \tag{25}$$

Using eqn (19), (21) and (25) we find condensation when the undersaturation satisfies

$$p - p_l^\dagger = 2\gamma_{lg}/(R_c - t_0) \quad \text{(cylinder)} \tag{26a}$$

where we have assumed $t_0 \gg \lambda^{-1}$. In other words, we recover the macroscopic expression (5*a*), but now the film thickness t_0 is determined self-consistently from eqn (21). We note that this analysis suggests that condensation should occur for undersaturations $p-p_l^\dagger$ that are considerably larger than the lower bound for metastable thick films described above. The corresponding result for the slit is

$$p - p_l^\dagger = 2\gamma_{lg}/(H - 2t_0) \quad \text{(slit)} \tag{26b}$$

with t_0 determined by eqn (22). We emphasize that both formulae are valid strictly in the limit of wide capillaries, small undersaturations and thick wetting films; they are not quantitatively accurate for most of the examples described in section 3. Indeed these formulae should prove more useful[6] in the study of the thick wetting films that occur in capillary rise experiments of the type performed recently by Moldover and Gammon.[29] Here the degree of undersaturation is determined by gravity and therefore can be made arbitrarily small. However, it is likely that van der Waals forces play a crucial role in these circumstances.[6] For a Yukawa fluid confined in a cylinder with a wall potential $V_{cvw}(R)$ given by eqn (A 4), the slab approximation predicts condensation at

$$p - p_l^\dagger = 2\gamma_{lg}/(R_c - 3t_0/2) \quad \text{(cylinder)} \tag{27a}$$

where the equilibrium thickness satisfies

$$t_0 = \left(\frac{p-p_l^\dagger - \gamma_{lg}/(R_c-t_0)}{2\varepsilon_w \sigma_w^2 \lambda_w^{-1}}\right)^{-\frac{1}{3}}. \tag{28}$$

Eqn (27*a*) and (28) remain valid for a Lennard-Jones 12–6 fluid confined by a van der Waals wall but the strength parameter in the denominator of eqn (28) is reduced.[6] The corresponding result for a slit with van der Waals walls is

$$p-p_1^\dagger = 2\gamma_{lg}/(H-3t_0) \quad \text{(slit)}. \tag{27b}$$

There is no simple macroscopic interpretation of eqn (27). Whilst $H-2t_0$ or R_c-t_0 may be regarded as the effective mean radius of curvature of the appropriate meniscus, $H-3t_0$ and $R_c-3t_0/2$ cannot. As recognized by Derjaguin,[8, 28] the corrections to the macroscopic formulae depend explicitly on the $-z^{-3}$ asymptotic decay assumed for the wall potential. Other algebraic decays will produce different corrections, *i.e.* if $V_p(z)$ decays as $-z^{-m}(m>2)$ for large z, the denominator in eqn (27*b*) and (27*a*) must be replaced by $H-2t_0-2t_0/(m-1)$ and $R_c-t_0-t_0/(m-1)$, respectively, with t_0 determined accordingly.

Eqn (28) again implies an implicit lower bound on the undersaturation; $p-p_1^\dagger$ must be greater than $\gamma_{lg}/(R_c-t_0)$. The results plotted in fig. 7 for $\lambda R_c = 20$ indicate that the limits of metastability of the 'gas' branch are similar for both types of wall potential.

We now turn to the application of the slab approximation to the determination of capillary critical points for fluids confined in cylinders. The corresponding analysis for a slit has already been described in detail.[5] From our numerical calculations, we find that in the neighbourhood of a critical point the coexisting density profiles $\rho(R)$ usually have similar shapes, but different central densities ρ_M. Often the profiles are quite flat. This suggests making the approximation $\rho(R)=\rho_M$ for $0 \leqslant R \leqslant R_c$. Such an approximation cannot account for wetting films, but these are not present[5] for the smaller radii and larger undersaturations which characterize the capillary critical points. The grand potential of the uniform slab is

$$\frac{\Omega(\rho_M)}{2\pi L} = \frac{R_c^2}{2}\left[f_h(\rho_M)-\frac{\alpha}{2}\rho_M^2-\mu\rho_M\right]+\frac{\rho_M}{2}R_c^2(\alpha\rho_M-4\varepsilon_w)I_1(\lambda R_c)K_1(\lambda R_c) \tag{29}$$

which has precisely the same dependence on ρ_M as that for the slit. The equilibrium ρ_M is that which minimizes Ω at fixed μ, T and R_c, *i.e.*

$$0 = [\mu_h(\rho_M)-\alpha\rho_M-\mu]+2(\alpha\rho_M-2\varepsilon_w)I_1(\lambda R_c)K_1(\lambda R_c). \tag{30}$$

In the limit $R_c\to\infty$, $I_1(\lambda R_c)K_1(\lambda R_c)\to 1/(2\lambda R_c)$ and the bulk density ρ_b is determined, as is usual, from the roots of $\mu=\mu_h(\rho_b)-\alpha\rho_b$. For finite R_c, the second term in eqn (30) becomes relevant and the roots of this equation differ from the bulk values. In particular, it is possible to choose μ to lie outside the bulk two-phase region and still obtain multiple roots of eqn (30). If two solutions with distinct values of ρ_M have equal values of Ω, they coexist. For a certain (critical) value of R_c, the multiple roots merge into a single critical value ρ_M^{cr}. The latter is equal to the bulk critical density ρ_c; ρ_M^{cr} is T and R_c independent in this slab approximation.[5] The critical radius R_c^{cr} satisfies

$$\frac{T}{T_c} = 1-2I_1(\lambda R_c^{cr})K_1(R_c^{cr}) \tag{31}$$

where T_c is the bulk critical temperature. For a given T this equation determines R_c^{cr}. Alternatively, it determines the capillary critical temperature T_c^{cap} for a given radius R_c. The corresponding formula[5] for the slit is

$$\frac{T}{T_c} = 1-\frac{[1-\exp(-\lambda H^{cr})]}{\lambda H^{cr}}. \tag{32}$$

In the limit $\lambda R_c \gg 1$, eqn (31) can be expanded as

$$\frac{T_c^{cap}}{T_c} = 1-\frac{1}{\lambda R_c}+\frac{3}{8(\lambda R_c)^3}+O\left(\frac{1}{\lambda R_c}\right)^5$$

so that the critical temperature is reduced below its bulk value by an amount inversely proportional to λR_c:

$$\frac{T_c - T_c^{cap}}{T_c} \approx \frac{1}{\lambda R_c}. \tag{33}$$

An equivalent shift, $1/\lambda H$, is obtained from eqn (32) in the limit $\lambda H \gg 1$. It is likely that neither result gives the correct asymptotic behaviour as $H \to \infty$ and $T_c^{cap} \to T_c$. The slab approximation omits the effects of bulk criticality. When these were properly included,[30] for a particular lattice-gas model the shift was proportional to $1/H^2$, as $H \to \infty$, in mean-field theory. However, for separations $\lambda H \leqslant 20$, and temperatures $T \leqslant 0.95 T_c$, eqn (32) provides a good account of the location of the capillary critical points calculated from the full theory for the slit.[5] A similar level of agreement is expected from eqn (31) for cylinders. Moreover we note that the variation of T_c^{cap} with a R_c predicted by eqn (31) is very close to the variation of T_c^{cap} with H predicted by eqn (32), even for values of λR_c and λH as small as 2. As is the case for slits,[5] the capillary critical points lie outside the bulk two-phase region [μ lies below the loop in $\mu(\rho)$] in the complete wetting regime $T > T_w$.

A slab approximation can also be used to investigate the prewetting transition described in section 3. Let the grand potential of the configuration with the (thick) wetting film of thickness t_α be $\Omega_\alpha(t_\alpha)$ and that with the (thin) film of thickness t_β be $\Omega_\beta(t_\beta)$. These configurations coexist in the pore when $\Omega_\alpha = \Omega_\beta$ or $\omega_\alpha^{ex} = \omega_\beta^{ex}$. Assuming that the grand potentials of both can be expressed in the form of eqn (23), it follows that coexistence (prewetting) occurs when

$$(p - p_l^\dagger)_{pw} = \left(\frac{\Delta\omega_\beta(t_\beta) - \Delta\omega_\alpha(t_\alpha)}{t_\alpha - t_\beta} + \gamma_{lg}/R_c\right)\left(1 - \frac{(t_\alpha + t_\beta)}{2R_c}\right)^{-1} \quad \text{(cylinder)}. \tag{34a}$$

(This is equivalent to assuming both films consist of metastable 'liquid' at density $\rho_l^\dagger$ and pressure $p_l^\dagger$.) If $t_\alpha \gg t_\beta$ we expect $(\Delta\omega_\beta - \Delta\omega_\alpha) > 0$, since this difference will depend mainly on a term $\lambda^{-1}(\varepsilon_w - \alpha\rho_l^\dagger/2)(\rho_l^\dagger - \rho_v)[\exp(-\lambda t_\beta) - \exp(-\lambda t_\alpha)]$ which is positive. For the slit the same approximations predict prewetting when

$$(p - p_l^\dagger)_{pw} = \frac{\Delta\omega_\beta(t_\beta) - \Delta\omega_\alpha(t_\alpha)}{t_\alpha - t_\beta} \quad \text{(slit)}. \tag{34b}$$

This undersaturation is very weakly H dependent; the difference $\Delta\omega_\beta - \Delta\omega_\alpha$ depends on terms such as $\exp[-\lambda(H - 2t)]$. Consequently the prewetting transition is shifted only slightly from its location at single wall ($H = \infty$), as was found[25] in our numerical calculations. In the cylinder, on the other hand, the undersaturation at which prewetting occurs is substantially increased by the term γ_{lg}/R_c in the numerator of eqn (34). This term again has its origin in the interfacial area contribution to $\omega^{ex}(t)$. Increasing t lowers this contribution; the balance of 'bulk' and 'surface' contributions is quite different between cylinders and slits and it is this which produces the striking difference in the shift of the prewetting transition shown in fig. 9. Within the same approximation scheme a triple point occurs when $(p - p_l^\dagger)_{pw}$, as estimated from eqn (34), is approximately equal to $2\gamma_{lg}/(R_c - t_\alpha)$ for the cylinder or $2\gamma_{lg}/(H - 2t_\alpha)$ for the slit. Thus,

$$R_{c\,triple} \approx t_\alpha + \gamma_{lg}\left(1 - \frac{t_\alpha}{R_c}\right)\frac{(t_\alpha - t_\beta)}{(\Delta\omega_\beta - \Delta\omega_\alpha)} \quad \text{(cylinder)} \tag{35a}$$

$$H_{triple} \approx 2t_\alpha + 2\gamma_{lg}\frac{(t_\alpha - t_\beta)}{(\Delta\omega_\beta - \Delta\omega_\alpha)} \quad \text{(slit)}. \tag{35b}$$

If we assume $t_\alpha \gg t_\beta$ and that the difference $\Delta\omega_\beta - \Delta\omega_\alpha$ is similar for slits and cylinders, it is clear that $R_{c\,triple}$ may be a factor of two, or more, smaller than H_{triple} for the same temperature.

In discussion prewetting and capillary critical points we have considered only exponentially decaying wall potentials as derived from the Yukawa model. For van der Waals wall potentials the corresponding analysis might produce rather different results.

5. Discussion

The results we have presented here complement those of our earlier study[5] of slits and support many of the conclusions we drew there. For small undersaturations a first-order transition from gas to metastable bulk liquid occurs with an accompanying jump in the adsorption. Such a transition is consistent with the classical, macroscopic description of capillary condensation as outlined in the introduction. If $T < T_w$ (partial wetting) the Kelvin equation [eqn (3*a*)] provides a rather accurate (good to a few percent) estimate of the condensation pressure, even for cylinders with radii as small as $10\ \lambda^{-1}$ (see fig. 5). Similar results were obtained for slits.[5, 31] For $T > T_w$, however, the deviations from the (unmodified) Kelvin equation [eqn (3)] are often very large and the condensation pressure can differ considerably between slits and cylinders. The deviations are especially pronounced at higher temperatures, although still well below T_c, where the adsorption on the 'gas' branch is large and the loops in Γ_m are shrinking (fig. 7). Under these circumstances the modified Kelvin equation [eqn (5)] is not particularly useful either. Indeed it is difficult to obtain a simple formula that is reliable for such cases. The self-consistent version [eqn (26)], obtained from the slab approximation, is accurate only when very thick films are present. This requires large radii and very small undersaturations, conditions that are not met in most adsorption measurements made on mesoporous solids, but which could be realized in capillary rise experiments.[6, 8, 28, 29] Eqn (21), (22) and (28) for the thickness of the film are useful, nevertheless, in providing a simple explanation of why metastable thick films can extend to much larger undersaturation ratios ρ_b/ρ_g in slits than in cylinders, something which might be relevant for the shape of the hysteresis loops in Γ_m.

As the radius is decreased, condensation is shifted to smaller undersaturation ratios and the loops in Γ_m shrink. The macroscopic description of capillary condensation is no longer applicable since one often finds condensation occurring for a chemical potential μ that falls outside the bulk two-phase region,[5] *i.e.* there is no metastable bulk liquid for that value of μ. The subsequent description of the first-order transition is intimately connected with the loop in Γ_m and in other interfacial quantities. In the case of the slit it was possible to make an equal area construction, in terms of certain variables, to obtain coexisting configurations.[5] For cylinders such a construction is not straightforward but the physical mechanism remains the same. We remark that there is no equal area construction for Γ_m or the excess, Γ_{ex}, in terms of μ or p or ρ_b. The vanishing of the loop in Γ_m^{ex} at a given T signals a capillary critical point. Although we have not attempted to determine in detail the line of critical points for cylinders, we expect this to be similar to that obtained for slits[5] (for the equivalent potential functions). That this should be the case is suggested by the results of the slab approximation discussed in section 4 and from a few comparisons of numerical results. Although the slab approximation fails as $R_c \to \infty$ and $T_c^{cap} \to T_c$, it becomes more reliable at lower temperatures when $R_c > \xi(T_c^{cap})$, the appropriate bulk correlation length. [Criticality of the fluid in the pore is characterized by a diverging local compressibility at the centre and the growth of long-ranged transverse (along the axis of the cylinder) correlations.][5] In the opposite limit $R_c \to d$, the hard-sphere diameter, the slab approximation for critical points also fails. Indeed the present local density treatment of short-ranged (hard-sphere) correlations becomes completely inadequate in this limit where excluded volume or packing considerations are crucially important. More sophisticated density functional treatments,[17] which do include short-ranged correlations, are currently being applied to this problem and to the analogous case of the slit. Preliminary results for the latter indicate that the effects of

packing or layering become significant for $H \approx 3d$ and influence the first-order transition. Moreover two-dimensional-like liquid-gas condensation occurs for $H < d$ and temperatures below the two-dimensional critical temperature. Even within the confines of mean-field-theory much further investigation is required before the gross features of the phase equilibria, including possible critical points, will be ascertained for very narrow pores. The additional complexities associated with fluctuation corrections are likely to be fearsome!

As mentioned in the introduction, Nicholson[12] performed lattice gas calculations for adsorption in cylinders. His results for the coverage as a function of pressure for different radii are similar to ours although he did not emphasize the importance of loops and metastable states so the origin of the critical radius that he determined was somewhat obscured. The capillary critical points that we describe here and calculate explicitly for slits,[5] have the same origin as those obtained by Nakanishi and Fisher[30] in a related study. These authors work in the magnetic analogue and choose to fix H and vary T rather than construct isotherms. Their paper concentrates on 'shifts' of the bulk critical temperature arising from confinement.

Our results for prewetting in cylinders warrant further comment. There are good reasons, associated with the relative ranges of wall–fluid and fluid–fluid attractive potentials, or with algebraic decay of forces[4, 22, 32] for expecting the wetting transition at a single planar wall to be first order, as obtained originally by Cahn[33] and Ebner and Saam.[34] Whilst much experimental and computational effort has gone into the search for prewetting the only experimental evidence stems from very recent light scattering measurements on solid spheres immersed in a binary liquid mixture[35] and the only computer simulation to detect prewetting is for a lattice gas.[36] Since many adsorption experiments employ solid material in a disperse form (particles) as a substrate and the distance between the surfaces of the particles is typically about 100 Å in a material such as graphon, it is of interest to enquire whether confining geometry has a significant role for the possible observation of the prewetting transition. The results presented in section 3, together with our earlier ones,[25] suggest that stable prewetting is unlikely to occur for fluids confined between plate-like particles unless the separation between the plates is very large. Capillary condensation will usually occur in preference to prewetting. For fluids confined in cylindrical pores, however, the prewetting transition occurs at smaller pressures (larger undersaturation) than at a planar wall and it should be possible to observe this transition in pores whose radii are about 30 or 40 molecular diameters. Its signature would be a jump in the adsorption of the magnitude indicated by the dashed vertical lines in fig. 9, but at $\rho' < \rho'_{\text{cond}}$, so that the subsequent condensation occurs between the thick film and the 'liquid'. Two jumps, accompanied by hysteresis, would constitute a clear indication of prewetting in confined geometry. At the triple point there would be only one jump. We do not attempt to draw the $(1/R_c, T, \Delta\mu)$ phase diagram here, but remark that this will have the same form as that shown in fig. 5 of ref. (25) (with $1/R_c$ replacing $1/H$) except that the stable prewetting surface should be increased in extent because the line of triple points is moved to larger values of $1/R_c$. Evidently our results have repercussions for computer simulations of solid–fluid adsorption. Most simulations confine the fluid between two adsorbing walls, *i.e.* in a slit with finite wall separation H. Usually $H \ll 40d$ so one would not expect to observe stable prewetting in grand canonical Monte Carlo simulations of the type performed, for example, by Lane *et al.*[37] Confining the fluid in a cylinder would certainly appear to be more favourable, although the values of $R_{c\,\text{triple}}$ that we estimate are still rather large. It is possible, of course, that a transition between metastable thick and thin films could be observed if condensation could be avoided in the simulation. An alternative procedure is to fix the number of molecules,[25] but this complicates the subsequent interpretation.

Given that curvature contributions have a significant effect on determining the shift of the prewetting transition it is natural to enquire what happens for fluids adsorbed on

the outside of a single closed cylinder or a sphere immersed in bulk. There is no capillary condensation now but thick wetting films can develop on the wall for $T > T_w$. The analysis of section 4 yields an excess grand potential:

$$\omega^{ex}(t) = \frac{1}{2R_c}(p-p_l^\dagger)(2R_c t+t^2)+\gamma_{lg}\frac{t}{R_c}+\Delta\omega(t) \tag{36}$$

for the cylinder. The grand potential associated with the liquid–gas interface now increases as the film thickness t increases; the interfacial area increases in this case. For the wall potential based on the Yukawa model the equilibrium thickness t_0 is given by

$$\lambda t_0 \approx -\ln\left(\frac{p-p_l^\dagger+\gamma_{lg}/(R_c+t_0)}{(\rho_l-\rho_g)(\varepsilon_w-\alpha\rho_l/2)}\right) \tag{37}$$

which should be constrasted with eqn (21). The curvature contribution $\gamma_{lg}/(R_c+t)$ now acts to increase the undersaturation $p-p_l^\dagger$. Thus, t_0 does not diverge in the limit $p \to p_{sat}$, provided R_c, the external radius, remains finite.[38] t_0 can, nevertheless, be large for small γ_{lg} and large R_c. The undersaturation at which prewetting occurs can be estimated by following the previous argument and we find

$$(p-p_l^\dagger)_{pw} = \left(\frac{(\Delta\omega_\beta-\Delta\omega_\alpha)}{t_\alpha-t_\beta}-\frac{\gamma_{lg}}{R_c}\right)\left(1+\frac{(t_\alpha+t_\beta)}{2R_c}\right)^{-1} \tag{38}$$

rather than eqn (34*a*). Consequently the transition is now shifted by roughly the same amount, but in the opposite direction, *i.e.* to smaller undersaturations than that appropriate to a single planar wall. The prewetting line $\Delta\mu_{pw}(R_c)$ slopes towards small $\Delta\mu$ as R_c is reduced. Eqn (38) suggests that there is a limiting radius below which prewetting does not occur. The same conclusion was reached by Levinson *et al.*[38] from analysis of the Cahn[33] model applied to fluids outside cylinders. Equivalent results hold for spheres; again the curvature effect shifts prewetting towards smaller $\Delta\mu$ making it difficult to observe except for rather large radii. Such observations may be relevant to experiment.[35]

We return finally to real porous solids and ask whether our results have consequences for the interpretation of adsorption measurements. Explanations of the observed hysteresis abound.[1, 3, 7] These often invoke the difference in shape of the meniscus between a 'full' and an 'empty' pore, an explanation we do not find satisfactory. For the idealised single cylindrical and slit-like pores considered here, the adsorption simply jumps vertically at the first-order transition. However, hysteresis could certainly be associated with the metastable portions of the loop in Γ_m. For example, in fig. 6 adsorption might occur along the path ABCD and desorption along DCEA, avoiding the unstable portions where $(\partial\Gamma_m/\partial\rho') < 0$. If desorption from 'liquid' to 'gas' occurs close to the equilibrium transition the resulting hysteresis loops would be similar to those found in measurements.[1] Such loops would also manifest themselves in computer simulations. It is tempting then to infer that the hysteresis found in experiment is associated with the mechanism described here. Presumably the non-uniformity of the pore size distribution and the complex connectivity of the pores in a real material act to smear out the hysteresis loops. That is not to say that certain pore geometries are not more important than others. (Conical and 'ink bottle' shapes are favoured in the literature!)[1] Our work suggests that metastable wetting films persist to much larger pressures in slit geometry than in cylindrical geometry and this could lead to broader hysteresis loops in the former. In the literature[1, 3, 7, 9] there is much confusion regarding the effect of pore geometry on hysteresis. It is sometimes suggested that certain geometries exhibit hysteresis, whilst others do not. We believe that such misconceptions arise from a failure to appreciate the underlying character of capillary condensation. Our

present interpretation of hysteresis is the same as that advanced many years ago by Hill[11] and is similar to that described by Saam and Cole.[13] It differs in detail from the explanations of hysteresis put forward by Derjaguin and Churaev,[28] although these authors also recognized the importance of the limit of metastability of wetting films.

An important prediction of the present work is that, for fixed radius, the jump in adsorption associated with condensation should decrease as T is increased and should vanish at a critical temperature T_c^{cap}. This is illustrated in fig. 8. Such behaviour would manifest itself in real porous materials as the shrinking and eventual disappearance of hysteresis loops with increasing T. The measured adsorption isotherms for certain systems certainly exhibit this trend. In particular recent data[39] for Xe on vycor glass and on activated carbon powder show the hysteresis loops shrinking and vanishing at $T/T_c \approx 0.87$ and 0.94, respectively. A detailed comparison of theory and experiment for these systems should provide a searching test of several of the ideas presented here.

We have benefitted from conversations and correspondence with D. H. Everett and M. M. Telo da Gama. Our collaboration was supported by an 'Acciones Integradas' grant from the British Council and the Spanish Ministry of Education.

Appendix 1

The effective one-body potential is

$$\phi_{\text{eff}}(\boldsymbol{r}) = -\alpha\lambda^3 \int \mathrm{d}\boldsymbol{r}'\, \rho(\boldsymbol{r}')\, \frac{\exp(-\lambda|\boldsymbol{r}-\boldsymbol{r}'|)}{4\pi\lambda|\boldsymbol{r}-\boldsymbol{r}'|} \tag{A 1}$$

with $\rho(\boldsymbol{r}') \equiv \rho(R') = 0$ for $R' > R_c$. For cylindrical geometry it is convenient to expand the Yukawa potential as follows:

$$\begin{aligned}\frac{\exp(-\lambda|\boldsymbol{r}-\boldsymbol{r}'|)}{|\boldsymbol{r}-\boldsymbol{r}'|} = \frac{1}{\pi}\int_{-\infty}^{\infty} \mathrm{d}k \cos(k\zeta) \sum_{m=-\infty}^{\infty} \exp(\mathrm{i}m\phi) \\ \times \{I_m(R(k^2+\lambda^2)^{\frac{1}{2}})\, K_m(R'(k^2+\lambda^2)^{\frac{1}{2}})\, \theta(R'-R) \\ + K_m(R(k^2+\lambda^2)^{\frac{1}{2}})\, I_m(R'(k^2+\lambda^2)^{\frac{1}{2}})\, \theta(R-R')\}\end{aligned} \tag{A 2}$$

where θ is the Heaviside (step) function, $\zeta = z - z'$ and ϕ satisfies

$$\begin{aligned}|\boldsymbol{r}-\boldsymbol{r}'| &= [|\boldsymbol{R}-\boldsymbol{R}'|^2 + (z-z')^2]^{\frac{1}{2}} \\ &= (R^2 + R'^2 - 2RR'\cos\phi + \zeta^2)^{\frac{1}{2}}.\end{aligned}$$

Using the relations

$$\frac{1}{2\pi}\int_{-\infty}^{\infty} \mathrm{d}\zeta \cos(k\zeta) = \delta(k)$$

and

$$\int_0^{2\pi} \mathrm{d}\phi \exp(\mathrm{i}m\phi) = \begin{cases} 2\pi & m = 0 \\ 0 & m \neq 0 \end{cases}$$

one finds

$$\begin{aligned}\int_{-\infty}^{\infty} \mathrm{d}\zeta \int_0^{2\pi} \mathrm{d}\phi\, \frac{\exp(-\lambda|\boldsymbol{r}-\boldsymbol{r}'|)}{|\boldsymbol{r}-\boldsymbol{r}'|} \\ = 4\pi[I_0(\lambda R)\, K_0(\lambda R')\, \theta(R'-R) + K_0(\lambda R)\, I_0(\lambda R')\, \theta(R-R')].\end{aligned} \tag{A 3}$$

Substituting this result into eqn (A 1) we obtain eqn (13).

Appendix 2

For van der Waals forces the wall–fluid potential is

$$V(\boldsymbol{r}) = -A \int \mathrm{d}\boldsymbol{r}' \frac{n_{\mathrm{w}}(\boldsymbol{r}')}{|\boldsymbol{r}-\boldsymbol{r}'|^6}$$

where $n_{\mathrm{w}}(\boldsymbol{r}')$ is the number density of wall molecules. In the cylindrical case the integral takes the form, for a constant density n_{w} in the cylinder,

$$V(\boldsymbol{r}) \equiv V_{\mathrm{cvw}}(R) = -An_{\mathrm{w}} \int \mathrm{d}\boldsymbol{R}' \int_{-\infty}^{\infty} \mathrm{d}z\,[(|\boldsymbol{R}-\boldsymbol{R}'|)^2+z^2]^{-3}.$$

The z integration, along the axis of the cylinder, is straightforward:

$$V_{\mathrm{cvw}}(R) = -\frac{3\pi}{8} An_{\mathrm{w}} \int_{|\boldsymbol{R}'| \geqslant R_{\mathrm{c}}} \mathrm{d}\boldsymbol{R}'\,(|\boldsymbol{R}-\boldsymbol{R}'|)^{-5}.$$

The remaining two-dimensional integral can be expressed as

$$V_{\mathrm{cvw}}(R) = -\frac{3\pi}{8} An_{\mathrm{w}}\, 2 \int_0^{\pi} \mathrm{d}\phi \int_{s(\phi)}^{\infty} \mathrm{d}t \frac{t}{t^5}$$

where $t = |\boldsymbol{R}'-\boldsymbol{R}|$ and $s(\phi)$ is a solution of $R_{\mathrm{c}}^2 = R^2+s^2-2Rs\cos\phi$. Thus

$$V_{\mathrm{cvw}}(R) = -\frac{\pi}{4} An_{\mathrm{w}} \int_0^{\pi} \frac{\mathrm{d}\phi}{s^3(\phi)}$$

with $s(\phi) = R\cos\phi \pm (R_{\mathrm{c}}^2 - R^2\sin^2\phi)^{\frac{1}{2}}$.

Introducing $x \equiv R/R_{\mathrm{c}}$ we rewrite this result as

$$V_{\mathrm{cvw}}(R) = -\frac{\pi An_{\mathrm{w}}}{4(R_{\mathrm{c}}-R)^3} Q(x)$$

with $$Q(x) = (1-x)^3 \int_0^{\pi} \mathrm{d}\phi\,[x\cos\phi \pm (1-x^2\sin^2\phi)^{\frac{1}{2}}]^{-3}.$$

Nicholson's[12] accurate polynomial fit to the function $Q(x)$ was employed in the calculations. The planar limit is recovered in the limits R and $R_{\mathrm{c}} \to \infty$ with $z = (R_{\mathrm{c}}-R) > 0$. This is achieved by setting $x = 1$; then $Q(1) = 2/3$ and $V_{\mathrm{cvw}}(z) = -\pi An_{\mathrm{w}}/6z^3$, as required. By inspection $Q(0) = \pi$, so that $V_{\mathrm{cvw}}(0) = -\pi^2 An_{\mathrm{w}}/4R_{\mathrm{c}}^3$.

The constant strength parameter An_{w} was fixed by requiring the integrated strength of the attractive planar potential to be the same as that obtained from the exponential model, *i.e.*

$$-\int_{\sigma_{\mathrm{w}}}^{\infty} \mathrm{d}z \frac{\pi}{6z^3} An_{\mathrm{w}} = -\int_0^{\infty} \mathrm{d}z\,\varepsilon_{\mathrm{w}} \exp(-\lambda_{\mathrm{w}} z) = -\frac{\varepsilon_{\mathrm{w}}}{\lambda_{\mathrm{w}}}$$

where σ_{w} is a measure of the molecular diameter. Then $An_{\mathrm{w}} = 12\varepsilon_{\mathrm{w}}\sigma_{\mathrm{w}}^2/\pi\lambda_{\mathrm{w}}$. Our final expression for the wall–fluid potential is

$$V_{\mathrm{cvw}}(R) = \begin{cases} -\dfrac{3\varepsilon_{\mathrm{w}}\sigma_{\mathrm{w}}^2}{\lambda_{\mathrm{w}}(R_{\mathrm{c}}-R)^3} Q(R/R_{\mathrm{c}}) & R < R_{\mathrm{c}}-\sigma_{\mathrm{w}} \\ \infty & R > R_{\mathrm{c}}-\sigma_{\mathrm{w}} \end{cases} \tag{A 4}$$

where we have restricted the fluid molecules to lie inside the radius $R_{\mathrm{c}}-\sigma_{\mathrm{w}}$, thereby avoiding the singularity at $R = R_{\mathrm{c}}$.

We note that an alternative expression for $V_{\mathrm{cvw}}(R)$ can be obtained in terms of a hypergeometric function.[13]

References

1 S. J. Gregg and K. S. W. Sing, *Adsorption, Surface Area, and Porosity* (Academic Press, New York, 1982), chap. 3.
2 A. Zsigmondy, *Z. Anorg. Chem.*, 1911, **71**, 356.
3 D. H. Everett and J. M. Haynes, in *Colloid Science, Vol. 1. Specialist Periodical Reports* (Royal Society of Chemistry, London, 1973), p. 123.
4 D. E. Sullivan and M. M. Telo da Gama, in *Fluid Interfacial Phenomena*, ed. C. A. Croxton (Wiley, New York, 1985).
5 R. Evans, U. Marini Bettolo Marconi and P. Tarazona, *J. Chem. Phys.*, in press.
6 R. Evans and U. Marini Bettolo Marconi, *Chem. Phys. Lett.*, 1985, **114**, 415.
7 L. H. Cohan, *J. Am. Chem. Soc.*, 1938, **60**, 433.
8 B. V. Derjaguin, *Zh. Fiz. Khim.*, 1940, **14**, 137 (English translation: *Acta Phys. Chem.*, 1940, **12**, 181.)
9 J. C. P. Broekhoff and J. H. de Boer, *J. Catal.*, 1967, **9**, 8.
10 D. Nicholson, *J. Chem. Soc., Faraday Trans. 1*, 1976, **72**, 29; D. Nicholson and N. G. Parsonage, *Computer Simulation and the Statistical Mechanics of Adsorption* (Academic Press, New York, 1982), chap. 7.4.
11 T. L. Hill, *J. Chem. Phys.*, 1947, **15**, 767.
12 D. Nicholson, *J. Chem. Soc., Faraday Trans. 1*, 1975, **71**, 239.
13 W. F. Saam and M. W. Cole, *Phys. Rev. B*, 1975, **11**, 1086.
14 D. J. Lee, M. M. Telo de Gama and K. E. Gubbins, *Mol. Phys.*, 1984, **53**, 1113.
15 B. Q. Lu, R. Evans and M. M. Telo da Gama, *Mol. Phys.*, 1985, **55**, 1319.
16 D. E. Sullivan, *Phys. Rev. B*, 1979, **20**, 3991.
17 P. Tarazona and R. Evans, *Mol. Phys.*, 1984, **52**, 847; P. Tarazona, *Phys. Rev. A*, 1985, **31**, 2672.
18 B. C. Freasier and S. Nordholm, *J. Chem. Phys.*, 1983, **79**, 4431, and references therein.
19 C. Ebner, W. F. Saam and D. Stroud, *Phys. Rev. A*, 1976, **14**, 2264.
20 R. Evans, *Adv. Phys.*, 1979, **28**, 143.
21 M. Abramowitz and I. A. Stegun, *Handbook of Mathematical Functions* (U.S. Dept. of Commerce, Washington, 1964), chap. 9.6.
22 P. Tarazona and R. Evans, *Mol. Phys.*, 1983, **48**, 799.
23 D. E. Sullivan, *J. Chem. Phys.*, 1981, **74**, 2604.
24 P. G. de Gennes, *J. Phys. (Paris)*, 1981, **42**, L377; R. Pandit, M. Schick and M. Wortis, *Phys. Rev. B*, 1982, **26**, 5112; M. P. Nightingale, W. F. Saam and M. Schick, *Phys. Rev. Lett.*, 1983, **51**, 1275; R. Lipowsky, *Phys. Rev. Lett.*, 1983, **52**, 1429.
25 R. Evans and U. Marini Bettolo Marconi, *Phys. Rev. A*, 1985, **32**, 3817.
26 W. van Megen and I. K. Snook, *Mol. Phys.*, 1985, **54**, 741.
27 J. Specovious and G. H. Findenegg, *Ber. Bunsenges. Phys. Chem.*, 1980, **84**, 690.
28 B. V. Derjaguin and N. V. Churaev, *J. Colloid Interface Sci.*, 1976, **54**, 157.
29 M. R. Moldover and R. W. Gammon, *J. Chem. Phys.*, 1984, **80**, 528.
30 H. Nakanishi and M. E. Fisher, *J. Chem. Phys.*, 1983, **78**, 3279, and references therein.
31 R. Evans and P. Tarazona, *Phys. Rev. Lett.*, 1984, **52**, 557.
32 *E.g.* R. Lipowsky and D. M. Kroll, *Phys. Rev. Lett.*, 1984, **52**, 2303; D. M. Kroll and T. F. Meister, *Phys. Rev. B*, 1985, **31**, 392; S. Dietrich and M. Schick, *Phys. Rev. B*, 1985, **31**, 4718; T. Aukrust and E. H. Hauge, *Phys. Rev. Lett.*, 1985, **54**, 1814; C. Ebner, W. F. Saam and A. K. Sen, *Phys. Rev. B*, 1985, **31**, 6134.
33 J. W. Cahn, *J. Chem. Phys.*, 1977, **66**, 3667.
34 C. Ebner and W. F. Saam, *Phys. Rev. Lett.*, 1977, **38**, 1486.
35 D. Beysens and D. Estève, *Phys. Rev. Lett.*, 1985, **54**, 2123.
36 C. Ebner, *Phys. Rev. A*, 1981, **23**, 1925.
37 J. E. Lane, T. H. Spurling, B. C. Freasier, J. W. Perram and E. E. Smith, *Phys. Rev. A*, 1979, **20**, 2147.
38 P. Levinson, J. Jouffroy and F. Brochard, *J. Phys. (Paris)*, 1985, **46**, L21.
39 D. H. Everett and S. Nuttal, personal communication.

Received 14*th August*, 1985